ADVANCED ENERGY MATERIALS
www.advenergymat.de

Host–Guest Complexation of α-Cyclodextrin and Triiodide Ions for Enhanced Performance of Ionic Thermoelectric Capacitors

*Shih-Ting Kao, Ching-Chieh Hsu, Shao-Huan Hong, U-Ser Jeng, Chia-Hsin Wang, Shih-Huang Tung, and Cheng-Liang Liu**

Ionic thermoelectric materials have emerged as a promising avenue for harvesting low-grade waste heat, with significant potential for applications in wearable electronics. This study introduces a novel design for ionic thermoelectric capacitors (ITECs) by incorporating host–guest complexation between α–cyclodextrin (α-CD) and triiodide ions (I_3^-). The strong host–guest complexation between α-CD and I_3^- confines the diffusion of I_3^- within the cylindrical cavities of α-CD, as evidenced by UV–vis spectroscopy and ^{13}C-NMR analysis. This confinement enhances the ion mobility difference between I_3^- and sodium ions, which in turn significantly boosts the ionic thermopower of the polyvinyl alcohol/α-CD/NaI hydrogels. Accordingly, the optimized sample achieves an impressive positive ionic thermopower of 14.24 mV K^{-1} and a high ionic power factor of 477.2 μW K^{-2} m^{-1}. Furthermore, the stretchable ITEC demonstrates a substantial power density of 5.9 mW m^{-2}. When integrated into a 3-leg device, a stable thermovoltage of 176 mV is generated under a temperature gradient of 4.4 K, thus highlighting the potential of this system for efficient thermal energy harvesting.

1. Introduction

The global energy crisis and increasing demand for renewable energy sources have highlighted the critical need for advances in ionic thermoelectric (i-TE) materials research.[1,2,3] These materials are capable of converting waste heat into electrical energy, thereby offering a promising strategy for reducing the present reliance on fossil fuels, mitigating carbon emissions, and promoting sustainability. Unlike conventional electronic thermoelectric (e-TE) materials,[4,5] which utilize electrons and holes in semiconductor materials as charge carriers, the i-TE materials rely on the diffusion of ions in liquid or gel electrolytes to facilitate charge transfer. A key advantage of i-TE materials is their significantly higher thermopowers of up to tens of millivolts per Kelvin, which is ≈10^2–10^3 times greater than that of e-TE materials,[6] thus making them particularly suited for recovering low-grade waste heat. Furthermore, i-TE materials are typically based on stretchable polymer gels, which offer properties such as flexibility, adhesion, biocompatibility, and lightweight design, thereby expanding their applicability.[7,8]

The i-TE materials can be divided into two main categories based on their power generation mechanisms, namely: i) thermogalvanic cells (TGCs) and ii) ionic thermoelectric capacitors (ITECs).[9,10] The TGCs generate voltage by exploiting the potential difference created between two electrodes subjected to a temperature gradient, where redox ion couples drive continuous power generation via a faradaic process. By contrast, the ITECs rely on the Soret effect, in which differential ion diffusion under a temperature gradient leads to a non-faradaic potential difference. This potential difference is typically larger than the voltage produced by the TGCs. In ITECs, the process induces the formation of an electric double layer on each electrode, so that the device functions similarly to a capacitor. Specifically, although the ions do not directly enter the electrodes to be conducted through the internal circuit, they enable charge and discharge via an external circuit, thereby mimicking the behavior of a capacitor.[11] The high sensitivity of this potential difference to temperature gradients further enhances the suitability of ITECs for thermosensing applications.[12,13]

S.-T. Kao, C.-C. Hsu, S.-H. Hong, C.-L. Liu
Department of Materials Science and Engineering
National Taiwan University
Taipei 10617, Taiwan
E-mail: liucl@ntu.edu.tw
U-S. Jeng, C.-H. Wang
National Synchrotron Radiation Research Center
Hsinchu 30076, Taiwan
S.-H. Tung, C.-L. Liu
Institute of Polymer Science and Engineering
National Taiwan University
Taipei 10617, Taiwan
C.-L. Liu
Advanced Research Center for Green Materials Science and Technology
National Taiwan University
Taipei 10617, Taiwan

The ORCID identification number(s) for the author(s) of this article can be found under https://doi.org/10.1002/aenm.202405502

DOI: 10.1002/aenm.202405502

The thermopower of an ITEC can be quantified by using Equation (1)[4]:

$$\text{Thermopower} = -\frac{V_H - V_C}{T_H - T_C} = \frac{n_+ D_+ S_+ - n_- D_- S_-}{e\left(n_+ D_+ - n_- D_-\right)} \quad (1)$$

where V_H and V_C represent the potential at the hot and cold ends, T_H and T_C denote the temperatures at the hot and cold ends, n_+ and n_- are the concentrations of cations and anions, D_+ and D_- are the diffusion coefficients of the cations and anions, S_+ and S_- represent the Eastman entropy of the cations and anions, and e is the elementary charge on the electron. To achieve a higher thermopower, it is crucial to maximize the differences in D and S between the cations and anions. Consequently, a significant portion of research on ITECs has focused on enhancing these differences by controlling electrostatic interactions,[14–17] van der Waals forces,[18] hydrogen bonds,[17,19] and other interactions between ions, polymers, solvents, and additional ionic species. For example, Zhao et al.[20] reported on a PEO/LiTFSI-EmimBF_4 ionogel that leveraged the coordination bonding between Li^+ ions and poly(ethylene oxide) (PEO) chains, as well as the ion-selective association between Li^+ and tetrafluoroborate (BF_4^-) to promote the formation of free trifluoromethanesulfonimide ($TFSI^-$) ions, thus resulting in an n-type ITEC. The PEO/LiTFSI-[Emim][BF_4] material exhibited a thermopower of −15 mV K^{-1} and an ionic conductivity (σ_i) of 1.86 mS cm^{-1}. Additionally, Hu et al.[21] introduced a CG-MA hydrogel based on chitosan grafted with melamine (MA), which utilized the chelating effect between MA and Fe^{3+} to achieve the ion separation required for ITECs. The CG-MA hydrogel achieved a thermopower of −7.24 mV K^{-1} and an impressive power density of 4.52 W m^{-2}.

Another effective approach for achieving ion separation in the ITEC is host–guest complexation. This is a key concept in supramolecular chemistry, and involves non-covalent interactions such as hydrogen bonding, or hydrophobic effects between a larger host molecule and a smaller guest molecule, to form a stable complex.[22,23] Typically, the host molecules (e.g., cyclodextrins (CD),[24] crown ethers,[25] or calixarenes[26]) possess cavities that are structurally complementary to the guest molecules in terms of shape, size, and functional groups, thereby enhancing their affinity. Among the various molecules used in host–guest complexation, CDs are particularly significant due to their macrocyclic structures, comprising 6–9 pyranose glucose units.[27] The CDs exhibit a strong ability to form inclusion complexes, which can modify the physicochemical properties of guest molecules. This encapsulation capability finds wide applications in drug delivery,[28] as well as in the food and cosmetics industries.[29] The hydroxyl groups on the outer surface of the CDs confer excellent hydrophilicity, thus leading to high solubility in water. Internally, CDs consist of six monosaccharide carbon rings connected by oxygen bridges, thus providing a high concentration of non-bonding electron pairs. This structure imparts the CDs with high electron density and Lewis base characteristics,[30] thereby enabling them to encapsulate substances with lower electron density or polarity than water, such as the I_3^- ions used in the present study,[31] thereby facilitating stable ion separation. This phenomenon was further elucidated by Okuda et al.,[32] who employed quantum mechanical calculations to simulate the specific inclusion of complex structures and molecular orbital distributions. Previous studies, such as the work on liquid TGCs utilizing α-CD to modulate the thermopower of the I^-/I_3^- system, achieved a thermopower of 2.0 mV K^{-1} and a figure-of-merit (ZT) value of 0.005,[33] the application of host–guest complexation in ITEC design remains largely underexplored.

In the present study, a polyvinyl alcohol (PVA)-based hydrogel is presented in which α-cyclodextrin (α-CD) is grafted onto the PVA chains using glutaraldehyde (GLA). This process forms a stretchable hydrogel that is subsequently immersed in an aqueous NaI solution. The host–guest complexation between α-CD and I_3^- ions results in the formation of a stable [α-CD-I_3^-] complex, which effectively limits I_3^- diffusion and achieves ionic separation, thus making the hydrogel suitable for use in a p-type ITEC. The interaction between α-CD and I_3^- is verified through a range of spectral analyses, including FTIR, ^{13}C-NMR, UV–vis spectroscopy, and XPS. By optimizing the α-CD content within the PVA/α-CD/I_3^- hydrogel and adjusting the NaI concentration, an exceptional thermoelectric performance is achieved, with a thermopower of 14.24 mV K^{-1} and a power factor of 477.2 μW K^{-2} m^{-1}. Additionally, a power density of 5.9 mW m^{-2} is obtained with an external resistance of 100 Ω. These results highlight the successful application of supramolecular chemistry in ITEC design, as well as the potential for further research and development in this area.

2. Results and Discussion

2.1. Spectroscopy Analyses

As shown schematically in Figure S1 (Supporting Information) and described in detail in the Experimental Section, the presented hydrogels for ITEC application are composed of a hydrophilic PVA matrix with varying concentrations of α-CDs grafted onto the PVA chains by using GLA as a crosslinker.[34,35] Subsequently, the cast hydrogels are soaked in NaI solution to allow the ions to facilitate ion penetration into the polymer network. The as-fabricated PVA/α-CD/NaI hydrogels are denoted hereafter as PVAα_x/I_y, where x represents the concentration of α-CD in the solution (ranging from 0 to 0.12 M), while y denotes the concentration of the NaI solution used. The polymer network design is shown schematically in **Figure 1a**, where the immobilization of α-CD molecules effectively prevents their diffusion within the hydrogel matrix. Due to the amphiphilic nature of α-CD, with a hydrophobic internal cavity and a hydroxyl-rich exterior, these molecules form stable host–guest complexes ([α-CD-I_3^-]) with I_3^- ions, thus restricting anion thermal diffusion.

Furthermore, the incorporation of α-CD weakens the hydrogen bonding between the PVA chains, thereby reducing their ability to stack in an ordered fashion and allowing the chains to disperse more effectively in the solvent, thereby exposing more hydroxyl groups. This phenomenon not only has a profound impact on the mechanical properties of the hydrogel but also promotes ion mobility by facilitating the hopping mechanism of Na^+ between the amorphous regions of the polymer network.[36] The I_3^- ions are essential for the thermoelectric performance of the hydrogel, and are generated during the soaking process via oxidation of I^- in the NaI solution. In the presence of dissolved oxygen in water,[37,38] the following reactions occur: $O_2 + 4I^- + 2H_2O \rightarrow 2I_2 + 4OH^-$, and $I^- + I_2 \rightarrow I_3^-$. The resulting I_3^- ions

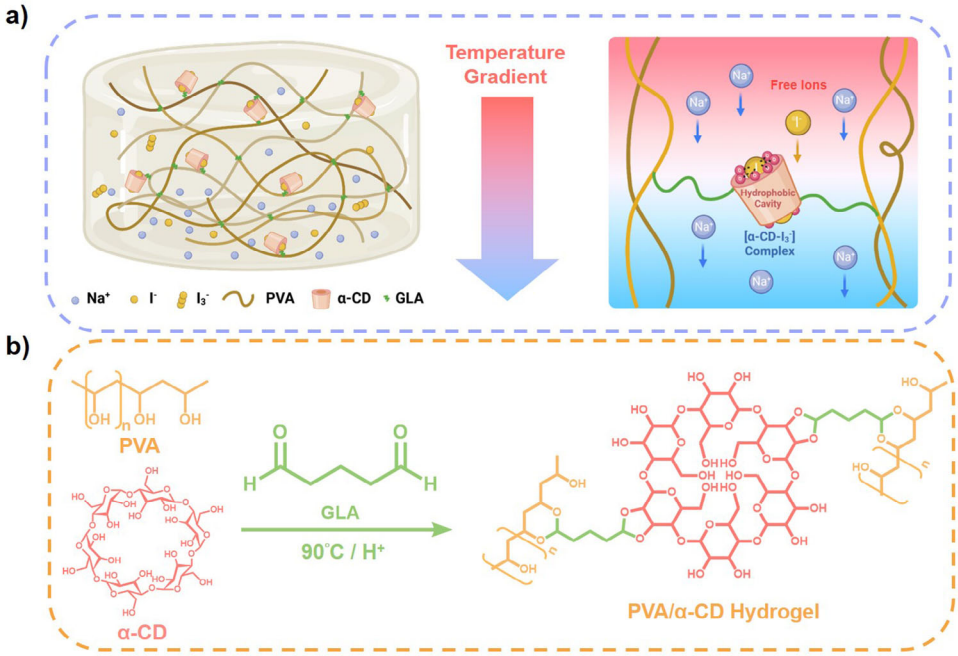

Figure 1. a) Schematic representation for the designed PVA/α-CD/NaI hydrogel. b) The synthesis pathway for PVA/α-CD hydrogel.

interact strongly with the α-CD, becoming encapsulated within its hydrophobic cavities. This encapsulation not only stabilizes the I_3^- ions but also drives the equilibrium toward further I_3^- formation in accordance with Le Chatelier's principle, which effectively minimizes the thermal diffusion of free I_3^- toward the cooler end of the thermoelectric hydrogel. This mechanism is crucial for enhancing the thermoelectric performance of the p-type ITEC, as it ensures selective cation diffusion, which is essential for efficient thermoelectric energy conversion.

The preparation of the PVA/α-CD polymer matrix involves the formation of an acetal structure via the acetalization reaction between two aldehyde groups of the GLA and adjacent hydroxyl groups on the α-CD rings and PVA chains. This reaction establishes covalent C—O bonds, which effectively crosslink the α-CD and PVA matrix via the GLA crosslinker,[34] as shown in Figure 1b. The success of this crosslinking reaction is confirmed by the FTIR spectra in **Figure 2**a. Thus, the FTIR spectrum of the PVA$\alpha_{0.12}/I_0$ hydrogel exhibits an absorption peak at ≈1134 cm^{-1}, which corresponds to the C—O—C stretching vibration of the acetal linkage.[39,40] Notably, this peak is absent from the spectra of both the pristine PVA and the pristine α-CD, thereby confirming the successful formation of acetal bonds in the crosslinked hydrogel. Furthermore, the complete FTIR spectra of the PVA, α-CD, and PVA$\alpha_{0.12}/I_0$ hydrogel (Figure S2, Supporting Information) exhibit variations in the O—H stretching region. Specifically, a blue shift in this absorption band is observed in the crosslinked hydrogel, which can be attributed to the reduction in hydrogen bonding.[41,42] This is likely due to the consumption of some O—H groups in the crosslinking reaction, as well as the disruption of the orderly arrangement of the PVA long chains. An additional absorption peak is observed near 2850 cm^{-1} in the PVA$\alpha_{0.12}/I_0$ hydrogel, corresponding to residual unreacted GLA.[40] This is likely a consequence of the reversible nature of the acetalization reaction involved in the crosslinking reaction. Notably, the remaining aldehyde groups within the hydrogel matrix are expected to facilitate the subsequent oxidation of I^- to I_3^- when the hydrogel is immersed in NaI solution, as described above.

The chemical structure of α-CD after crosslinking, and the coordination between α-CD and I_3^-, are elucidated by the ^{13}C–NMR spectra of the pristine PVA, the PVA$\alpha_{0.12}/I_0$, and the PVA$\alpha_{0.12}/I_{0.3}$ samples in Figure 2b. Here, characteristic signals corresponding to PVA are prominently observed in the 65–69 ppm region. Additionally, signals associated with the carbon atoms of α-CD[43] are detected in the PVA$\alpha_{0.12}/I_0$ and PVA$\alpha_{0.12}/I_{0.3}$ samples. Moreover, a significant decrease in the intensity of the α-CD peak is observed in the PVA$\alpha_{0.12}/I_{0.3}$ relative to the PVA$\alpha_{0.12}/I_0$, thereby suggesting that I_3^- ions become encapsulated within the hollow structure of α-CD in the PVA$\alpha_{0.12}/I_{0.3}$ sample, where the ionic charges exert a shielding effect on the magnetic field. This shielding weakens the local magnetic environment around the carbon atoms of α-CD, thereby reducing the signal intensity. Furthermore, Figure 2c highlights the signal corresponding to the C^2—O—H groups of α-CD, which provide reactive sites for acetal formation. This signal shows an overall downshift as the α-CD content increases, which is attributed to the stronger electron-withdrawing effect of the newly formed crosslinked C—O—C bonds compared to the original C—O—H bonds in the α-CD. The observed peak splitting at higher α-CD concentrations indicates the possibility of incomplete reactions, thus resulting in two distinct molecular environments for C^2 on α-CD. In addition, Figure 2d,e compare the chemical shifts of C^1 and C^6 in the PVA/α-CD hydrogels before and after NaI immersion. Upon the introduction of I_3^- into the hollow cavity of α-CD to form the host–guest complex, the vacant d orbitals of I_3^- form coordination bonds with the lone electron pairs on the oxygen atoms

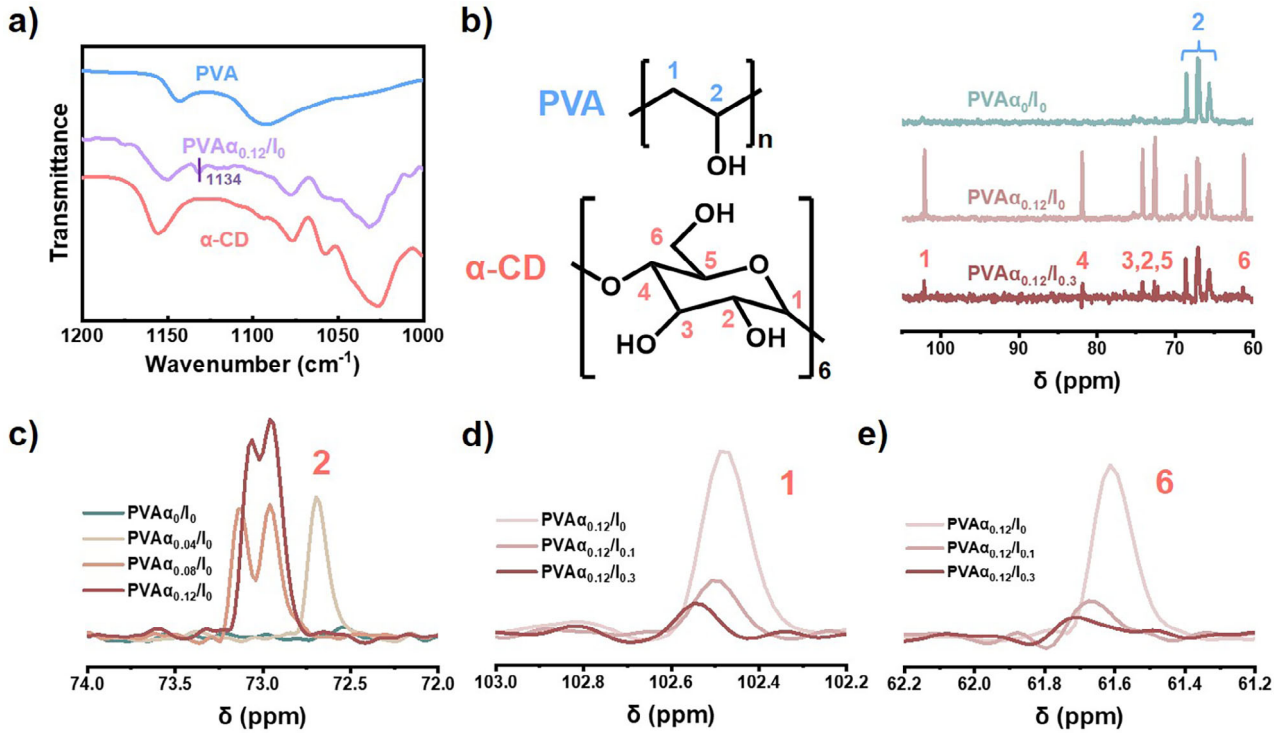

Figure 2. Spectral characterizations of PVA/α-CD/NaI hydrogels with different compositions. a) FTIR spectrum of pristine PVA powder, α-CD powder, and PVA$\alpha_{0.12}/I_0$ sample. b) Labels for each carbon of PVA and α-CD, and ^{13}C-NMR spectrum for PVAα_0/I_0, PVA$\alpha_{0.12}/I_0$ and PVA$\alpha_{0.12}/I_{0.3}$ sample. c–e) ^{13}C-NMR spectra for different PVA/α-CD/NaI hydrogel sample: c) C^2 of α-CD, d) C^1 of α-CD, e) C^6 of α-CD.

adjacent to C^1 and C^6. This interaction slightly reduces the electron cloud density around the carbon atoms, thus leading to the observed downshifting of the chemical shift in the ^{13}C-NMR spectra.

The formation of the [α-CD-I_3^-] host–guest complex is further confirmed by the UV–vis absorption spectra in **Figure 3**. Thus, the absence of characteristic absorption peaks due to the I_3^- ion at ≈288 and 352 nm[44] in the UV–vis spectrum of the PVA$\alpha_0/I_{0.3}$ sample (Figure 3a) clearly indicates that iodine is not present in this form in the absence of α-CD. However, as the α-CD content increases, the absorbances due to I_3^- also increase, thereby indicating a shift in the anion composition from freely migrating I^- ions in solution to I_3^- ions encapsulated within the α-CD. This encapsulation alters the diffusion behavior, thus resulting in a differential ion mobility between anions and cations. Furthermore, a comparison of the UV–vis absorption spectra of the PVAα_0/I_0, PVA$\alpha_0/I_{0.3}$, PVA$\alpha_{0.04}/I_0$, and PVA$\alpha_{0.04}/I_{0.3}$ samples (Figure 3b) indicates that a significant increase in the I_3^- content only occurs for the PVA$\alpha_{0.04}/I_{0.3}$ sample, where both α-CD and NaI are present in the hydrogel. This observation further demonstrates that the formation of I_3^- is facilitated by the host–guest complexation between α-CD and I_3^-, thereby supporting the role of α-CD in enhancing the selective anion-cation diffusion behavior within the hydrogel matrix.

Deeper insights into the coordination behavior between I_3^- and α-CD are provided by the XPS analysis in Figure 3c–f. Thus, the I $3d_{5/2}$ XPS spectrum of the PVA$\alpha_0/I_{0.3}$ sample exhibits two peaks at 618.5 and 620.6 eV, corresponding to the I^- and I_3^- ions, respectively.[45] In the PVA$\alpha_{0.12}/I_{0.3}$ sample, however, the I_3^- signal undergoes a significant shift to lower binding energy at 619.9 eV. This is attributed to the role of I_3^- as an electron acceptor in the coordination process with α-CD, where the increased electron density results in a redshift of its XPS signal. Conversely, the oxygen atoms in α-CD are regarded as electron donors in this coordination interaction. Consequently, a blueshift in the C—O signal is observed in the C 1s XPS spectrum of the PVA$\alpha_{0.12}/I_{0.3}$ compared to that of the PVA$\alpha_{0.12}/I_0$. This interpretation aligns with the findings derived from the above ^{13}C-NMR analysis.

Taken together, the above FTIR, ^{13}CNMR, UV–vis, and XPS analyses provide compelling evidence for the successful chemical cross-linking within the PVA/α-CD/NaI hydrogel. In addition, the coordination mechanism between α-CD and I_3^- has been elucidated, thereby demonstrating the feasibility of [α-CD–I_3^-] complex formation within the hydrogel matrix. As a p-type ITEC, the PVA/α-CD/NaI hydrogel predominantly forms stable [α-CD-I_3^-] coordination complexes, which effectively confine I_3^- ions within localized α-CD on the PVA chain. Meanwhile, Na^+ ions serve as the primary charge carriers, diffusing along the temperature gradient. Following this initial characterization, the microstructures and mechanical properties of the PVA/α-CD/NaI hydrogels will be explored in the following paragraphs.

2.2. Microstructure and Mechanical Properties

First, the microporous structures of the freeze-dried PVA/α-CD/NaI hydrogels are revealed by the SEM images in Figure S3

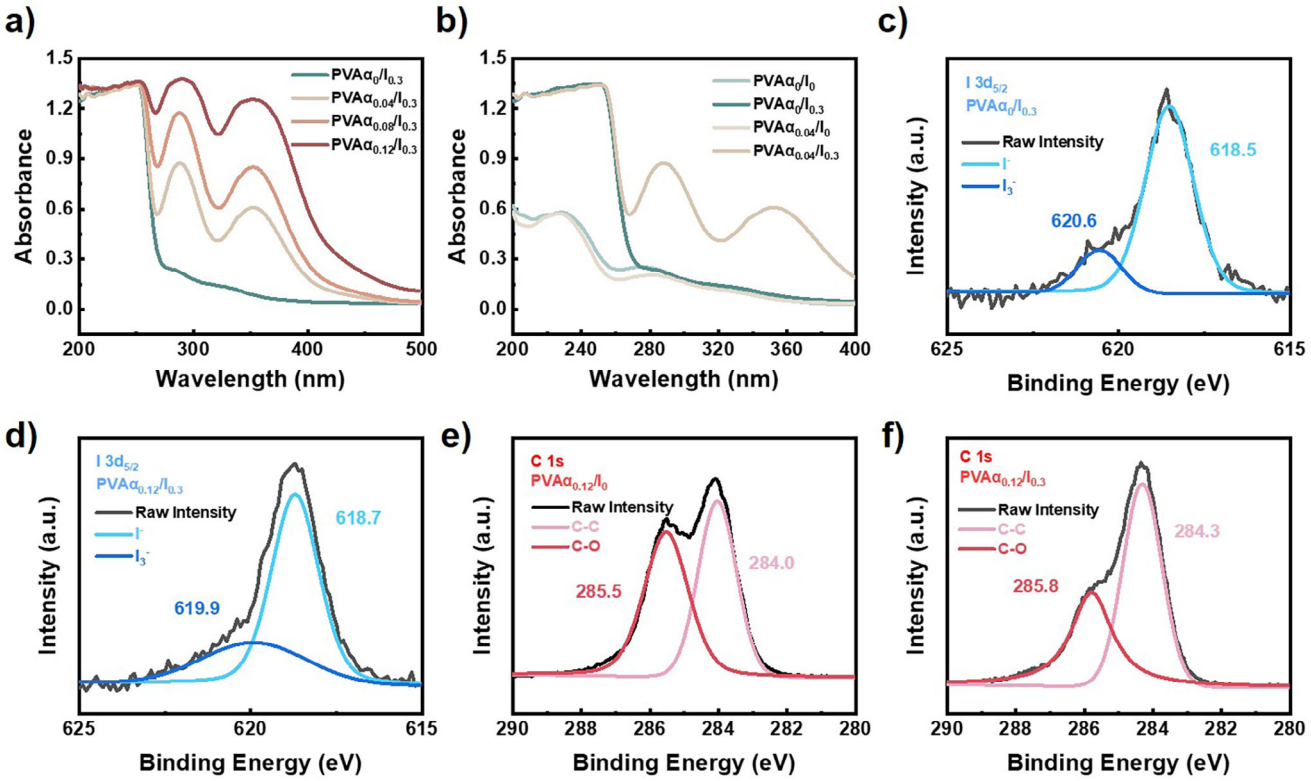

Figure 3. Spectral characterizations of PVA/α-CD/NaI hydrogels with different compositions. a,b) UV–vis spectra of each PVA/α-CD/NaI hydrogels sample. c,d) XPS I $3d_{5/2}$ signals for c) PVA$\alpha_{0/}I_{0.3}$, d) PVA$\alpha_{0.12/}I_{0.3}$. e,f) XPS C 1s signals for e) PVA$\alpha_{0.12/}I_{0}$, f) PVA$\alpha_{0.12/}I_{0.3}$.

(Supporting Information). This can be attributed to the sublimation of crystallized water under the applied low temperatures and high vacuum conditions. This observation suggests that the PVA/α-CD/NaI hydrogels possess dense and interconnected water channels, which are potentially beneficial for σ_i. Additionally, the network structure of PVA is also expected to enhance the stretchability and toughness of the material. However, the SEM results only reveal micron-sized structures, and these structures may have been slightly changed during the freeze-drying process. To adequately describe the microstructure of the hydrogels under ambient (hydrated) conditions, SAXS and XRD analyses are required in order to quantitatively elucidate the impact of α-CD incorporation on the microstructures of the PVA/α-CD/NaI hydrogels. During the SAXS measurements, the hydrogel samples are fully hydrated, which allows the results to accurately reflect the true microstructures of the hydrogels. To characterize the microstructures at different length scales, the scattering intensity I(q) is plotted against the scattering vector (q) on a double logarithmic scale, and the power law is applied to both the low-q and high-q regions, as shown in **Figure** 4a. The slope of the curve in these regions corresponds to the fractal dimension of the structure. In the high-q region, all of the samples follow the law I(q)–$q^{-1.8}$, which corresponds to a mass fraction of dimension 1.8.[46] This low fractal dimension suggests that, at the nanometer scale, the PVA chains and α-CD form loose, open aggregates, where the amorphous regions expand due to swelling in the solvent. The characteristic length of this aggregate can be determined using the Lorentzian model, based on Equation (2):

$$I(q) = \frac{I_0}{\left[1 + (q\xi)^2\right]} + \mathrm{Bgd} \quad (2)$$

In this model,[47] the coefficients I_0, background (Bgd), and the Lorentzian characteristic length (ξ) are obtained through fitting, with the Lorentzian exponent fixed at 2. The first term in the equation describes the local structure of the polymer segments, which is closely related to the interactions between the segments and the solvent, and refers to the size of the polymer-rich aggregates.

The Lorentz model fitting results are presented in Figure 4b and Table S1 (Supporting Information). As the α-CD content increases from 0 to 80 mM, the ξ is seen to increase from 82 to 120 Å. This is attributed to the insertion of α-CD between the PVA chains, which hinders the local stacking for the formation of crystalline regions and increases the quantity of amorphous regions to be swollen by solvent molecules, as shown schematically in Figure S4 (Supporting Information). In the low-q region, however, the power law exponent is ≈2.2, thereby indicating a mass-fractal structure[48] clustered with the PVA/α-CD aggregates at scales larger than several tens of nanometers. This suggests a self-similarity in the structural characteristics at various levels of observation.[49] Additionally, the temperature-variation SAXS results in Figure S5 (Supporting Information) indicate that the

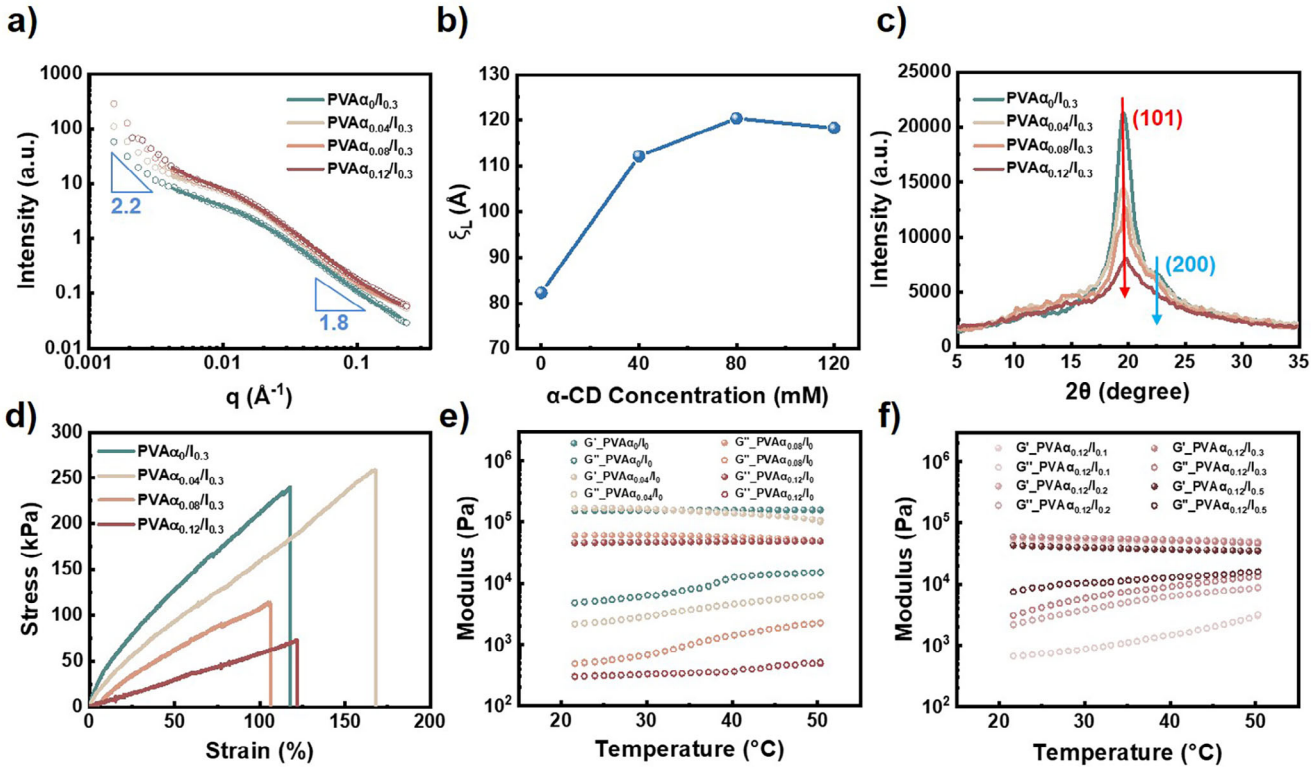

Figure 4. Microstructural and mechanical properties characterizations among different composition of PVA/α-CD/NaI hydrogel samples. a) SAXS data of each sample under ambient conditions. b) Lorentzian correlation length of each sample with different α-CD concentration. c) XRD spectra of different each sample with different α-CD concentration. d) Stress-strain curves of each sample with different α-CD concentration. e,f) Dynamic mechanical analysis indicating the storage modulus (G′) and loss modulus (G″) of each sample at varying temperatures.

PVA$\alpha_{0.12}$/I$_{0.3}$ hydrogel sample exhibits no significant differences in either the low-q or high-q regions across the temperature range of 20–40 °C. This demonstrates that the structures of the PVA/α-CD/NaI hydrogels are thermally stable within its operational temperature range.

The crystallinities of the PVA and α-CD are revealed by the XRD spectra in Figure 4c. Here, the diffraction peaks at 19.5° and 22.7° correspond to the respective (101) and (200) crystal planes of PVA.[50] With the introduction of the large α-CD molecules into the PVA polymer matrix, the intensities of these peaks gradually decrease, and the (200) peak of the PVA$\alpha_{0.12}$/I$_{0.3}$ sample nearly disappears. This suggests that the incorporation of α-CD inhibits the crystallization of PVA, particularly by disrupting the packing along the hydroxyl side chains of PVA. These XRD findings further support the increase in ξ observed in the high-q region of the SAXS results. This reduction in crystallinity further affects the mechanical properties, as discussed in the following paragraphs.

To quantify the impact of α-CD on the mechanical properties, the stress-strain curves of the hydrogels with varying α-CD contents are presented in Figure 4d, and the corresponding elastic moduli and toughnesses are summarized in Table S2 (Supporting Information). Thus, as the α-CD content is increased from 0 to 0.12 wt.%, the elastic modulus decreases from 211.4 to 57.7 kPa. This softening is attributed to the disruption of PVA crystallite formation due to the introduction of α-CD, as demonstrated by the XRD results. Hence, in this study, the maximum α-CD concentration was set at 0.12 M to prevent a substantial loss of structural integrity and ensure adequate mechanical strength. In terms of stretchability, the highest strain at breaking point is observed in the PVA$\alpha_{0.04}$/I$_0$ sample (Figure 4d), while the further addition of α-CD lowers the stretchability. A small amount of α-CD increases the proportion of amorphous regions, thereby extending the strand length between cross-linking points and enhancing the maximum strain at the breaking point. However, excessive α-CD leads to a significant reduction in crosslinking density, including both the chemical crosslinking between PVA chains mediated by GLA and the physical crosslinking of PVA crystallites, which deteriorates the network integrity and negatively affects the stretchability. Meanwhile, changing the concentration of NaI in the post-soaking step does not show any significant effect on the mechanical properties of the hydrogel, as demonstrated in Figure S6 (Supporting Information).

The dynamic rheological measurements in Figure 4e,f provide information on the storage modulus (G′) and loss modulus (G″) values of each sample across the temperature range of 20–50 °C. For all of the samples, the G′ values are consistently greater than the G″ values, which indicates that the hydrogel exhibits a more solid-like rheological behavior within its operational temperature range. As shown in Figure 4e, both G′ and G′′ decrease as the concentration of α-CD increases, which is consistent with the tensile test results. Meanwhile, Figure 4f reveals that the G″ varies slightly depending on the NaI concentration used during the soaking process. Due to the high osmotic pressures of the NaI solutions, the hydrogels undergo slight

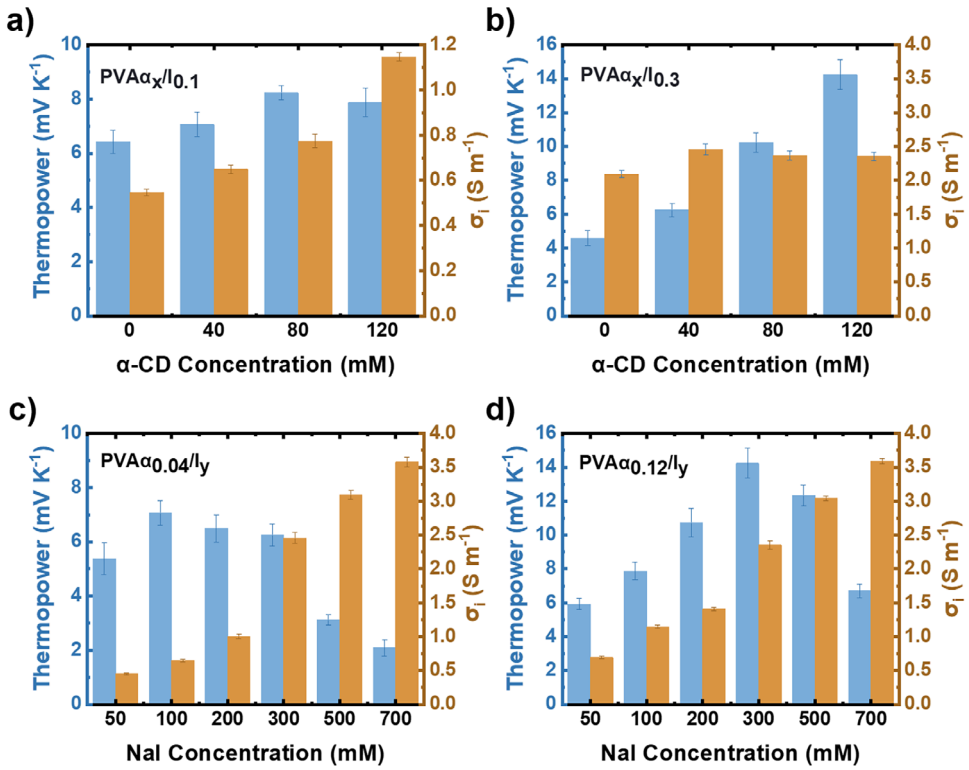

Figure 5. Thermopower and ionic conductivity(σ_i) for PVA/α-CD/NaI hydrogel samples with different compositions: a) PVAα_x/I$_{0.1}$, b) PVAα_x/I$_{0.3}$, c) PVA$\alpha_{0.04}$/I$_y$, d) PVA$\alpha_{0.12}$/I$_y$.

dehydration, which causes water molecules to diffuse out upon soaking. This results in a decrease in the swelling ratio of the hydrogels, where the PVA strands experience less extension and consequently become more flexible. Due to the increased mobility of the PVA strands, the samples soaked in higher concentrations of NaI exhibit a more liquid-like behavior, as revealed by a smaller difference between their G′ and G″ values. In summary, although the introduction of α-CD reduces both the elastic modulus and mechanical strength, the material remains capable of being bent. The excellent tensile strength of the PVA$\alpha_{0.12}$/I$_{0.3}$ hydrogel is demonstrated in Figure S7 (Supporting Information), where the material is seen to be capable of lifting a 600 g weight.

2.3. Thermoelectric Performance

Based on the experimental results in Section 2.1, which confirm the strong interaction between α-CD and I_3^-, it is anticipated that increasing the amount of confined I_3^- will further enhance the thermopower of PVA/α-CD/NaI hydrogel. In the following section, the thermopower of each hydrogel is measured by varying the ΔT across the two ends of the sample, plotting the resulting ΔV against the temperature difference, and obtaining the slope of the linear regression, as shown in Figure S8 (Supporting Information), where all of the tested hydrogel samples exhibit p-type thermoelectric behavior. The thermopower of each PVA/α-CD/NaI hydrogel sample is shown in Table S3 (Supporting Information). The effects of varying the α-CD concentration on the thermopower and σ_i of the PVAα_x/I$_{0.1}$ and PVAα_x/I$_{0.3}$ hydrogels are shown in **Figure** 5a,b. Thus, when the NaI concentration is maintained at 100 mM, the thermopower reaches a maximum of 8.24 mV K^{-1} at an α-CD concentration of 80 mM (Figure 5a). Increasing the α-CD concentration beyond this does not further enhance the thermopower, possibly because 80 mM of α-CD is sufficient to restrict all the I_3^- ions within the hydrogel matrix. However, when the NaI concentration is increased to 300 mM, the thermopower clearly increases with higher α-CD concentrations, reaching a maximum of 14.24 mV K^{-1} at 120 mM α-CD. This suggests that, in hydrogels with a fixed concentration of Na^+ and I^- ions, increasing the α-CD content confines increasing quantities of I^- ions, thereby achieving higher thermopowers. With respect to the σ_i of each sample, when the hydrogels are immersed in 100 mM NaI, an increase in α-CD content leads to a significant improvement in σ_i, up to a maximum of 1.15 S m^{-1} (Figure 5a). This is likely due to the disruption of crystallization between the PVA chains, as the bulky α-CD molecules hinder PVA stacking, thereby reducing crystallization and expanding the amount of loose amorphous regions. This structural change reduces polymer hindrance, thereby improving ion mobility. By contrast, for hydrogels with a higher NaI concentration of 300 mM (Figure 5b), this effect is less pronounced. At higher salt concentrations, ionic interactions dominate over the influence of polymer-chain crystallization, thus limiting the contribution of α-CD to increased σ_i. Therefore, the σ_i is less affected by the α-CD content when the NaI concentration is increased.

The effects of various NaI concentrations on the thermopower and σ_i of the hydrogels with fixed α-CD concentrations of 40 and 120 mM are presented in Figure 5c,d, respectively. In both

cases, increasing the NaI concentration generally leads to an increase in thermopower. For the hydrogel with 40 mM α-CD (Figure 5c), the thermopower peaks at 7.06 mV K^{-1} after soaking in 100 mM NaI solution. For the 120 mM α-CD hydrogel (Figure 5d), however, the maximum thermoelectric potential is 14.24 mV K^{-1} after soaking in 300 mM NaI solution. This indicates that when the α-CD content is fixed, the thermopower gradually increases as the NaI concentration increases until the concentration of the [α-CD-I_3^-] inclusion complex reaches chemical equilibrium and saturation. Beyond this point, further increases in NaI concentration result in excess I^- ions that are not encapsulated by α-CD. These free I^- ions continue to undergo thermodiffusion, along with the Na^+ ions, but do not contribute optimally to the thermopower, thus leading to a plateau or decrease in performance.

The variations in thermopower for hydrogels incorporating the same concentrations of different types of cyclodextrins, each with different internal diameters, after immersion in the same concentration of NaI, are shown in Figure S9a (Supporting Information). These results indicate that a substantial increase in thermopower is observed only with α-CD, where the thermopower reaches its maximum value. By contrast, replacing α-CD with β-CD or γ-CD, both of which possess larger internal cavities, leads to a marked decrease in thermopower to 3.85 and 4.22 mV K^{-1}, respectively. This indicates that the larger cyclodextrins are less effective in forming host–guest complexes with I_3^- ions. The specificity of α-CD in coordinating with I_3^- is attributed to its optimal cavity size, which facilitates stronger and more stable host–guest interactions with the I_3^- ions. Moreover, when NaI is replaced by NaCl to serve as a control group, the thermoelectric power of the α-CD-based hydrogel remains relatively stable at ≈11 mV K^{-1}, with no significant changes depending on the concentration of α-CD (Figure S9b, Supporting Information). These results suggest that the host–guest complexation between α-CD and I_3^-, which enhances the thermoelectric potential in the NaI system, does not occur with Cl^- ions. The NaCl system relies on ionic interactions that lack the selective coordination seen between α-CD and certain anions. When combined with the abovementioned UV–vis and ^{13}C–NMR spectroscopy results, it becomes clear that the strong host–guest complexation interaction between α-CD and I_3^- is critical for enhancing the performance of the p-type thermoelectric hydrogels. Compared to ITEC systems that depend on weaker van der Waals interactions between chains and ions, the α-CD and I_3^- complexation offers a stronger and more reliable mechanism for improving the thermoelectric properties. This highlights the feasibility of employing the [α-CD-I_3^-] complex as a key component for optimizing the thermopower in such systems.

Additionally, the thermal conductivity of the hydrogel is a crucial factor for determining the ionic figure-of-merit (ZT_i) value and, hence, the efficiency, of the PVA/α-CD/NaI hydrogel system. The ZT_i is obtained using Equation (3):

$$ZT_i = \frac{S_i^2 \sigma_i T}{\kappa} \tag{3}$$

where S_i represents the thermopower, T denotes the surrounding temperature, and κ is the thermal conductivity. Because the ZT_i is inversely proportional to the thermal conductivity, a lower thermal conductivity leads to a higher ZT_i, thereby improving the thermoelectric performance. In this system, the water content is ≈90% by weight, meaning that the thermal conductivity of each sample is close to that of water, which has a theoretical value of 0.60 W m^{-1} K^{-1}.[51] As the α-CD concentration increases, the crystallinity of the PVA polymer chains decreases, thus leading to more amorphous regions and a higher degree of swelling. This structural change results in a thermal conductivity that approaches that of water, as illustrated in Figure S10 (Supporting Information). Meanwhile, the ionic power factor (PF_i) of the hydrogel system can be calculated using Equation (4):

$$PF_i = S_i^2 \sigma_i \tag{4}$$

Thus, considering both the thermopower and the σ_i of each sample, it is essential to maximize the proportion of α-CD in the hydrogel, while matching it with an appropriate NaI concentration, in order to optimize the PF_i value. Based on the experimental results in Figure S11 (Supporting Information), the PVA$\alpha_{0.12}$/$I_{0.3}$ sample exhibits the highest PF_i value of 477.2 μW m^{-1} K^{-2}, along with a ZT_i value of 0.244. To demonstrate the potential for PVA$\alpha_{0.12}$/$I_{0.3}$ hydrogel presented in this work, its thermopower and power factor are compared with those of the previously reported ITEC materials utilizing a coordination complexation mechanism (Figure S12, Supporting Information).[52–54] This result highlights the exceptional thermoelectric properties of the PVA/α-CD/NaI hydrogel system, which are achieved without the use of ionic liquids or heavy metals. In view of these results, the following evaluations are focused on the PVA$\alpha_{0.12}$/$I_{0.3}$ sample, as this represents the optimal thermoelectric efficiency for the p-type ITEC.

To quantify the electrical energy generated by the ITEC, a four-stage charge–discharge test using the PVA$\alpha_{0.12}$/$I_{0.3}$ sample was conducted. The operating mechanism of the ITEC relies on selective ion diffusion, which facilitates charge separation and the formation of an electric double layer at each electrode, thus enabling energy storage. As shown in **Figure 6a**, the thermoelectric charge-discharge process of the ITEC is divided into four distinct stages. In Stage I, a temperature gradient of 4 K is applied across the device in order to drive the diffusion of ions, primarily Na^+, from the hot side to the cold side. This ion movement results in a potential difference (ΔV) of <0 between the hot side (V_{hot}) and the cold side (V_{cold}), which increases until a steady-state potential of −53 mV is reached. This indicates the completion of ionic diffusion across the temperature gradient. In Stage II, a variable resistor is introduced to connect the two electrodes, thus allowing electrons to flow between the electrodes via the external circuit from the lower potential to the higher potential. As a result, the voltage gradually decreases toward zero, as the potential between the electrodes equilibrates. The rate of this decay is dependent on the value of the external resistance, as demonstrated by the charging profiles under different resistances in Figure 6b. At the conclusion of this stage, the thermoelectric charging of the ITEC is complete. In Stage III, the external resistor is removed to form an open circuit, and the applied temperature gradient is immediately eliminated. Consequently, the ions within the hydrogel redistribute toward their initial, uniformly dispersed, state. However, the electrons and holes that were transferred during Stage

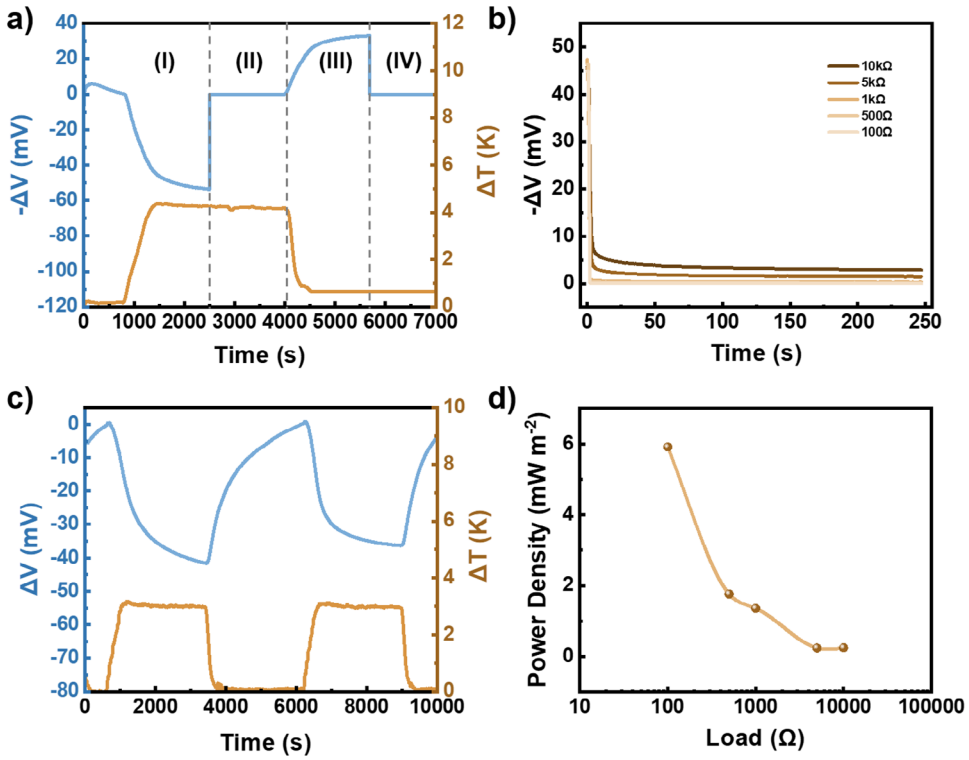

Figure 6. Thermoelectric performance of PVA$\alpha_{0.12}$/$I_{0.3}$ hydrogel sample. a) Voltage-time profile during four-stage charge-discharge test. b) Voltage–time profile for varying temperatures. c) decay curves under different external loads during stage II. d) the calculated average power density under different external loads during stage II.

II remain localized on the respective electrodes, thereby generating a potential difference with the opposite polarity to that observed in Stage I. Finally, in Stage IV, the electrodes are reconnected, thus allowing the stored charges to discharge through the external circuit. This completes the full charge–discharge cycle.

As shown in Figure 6a the reverse equilibrium voltage in Stage III does not completely correspond to the voltage measured in Stage I, thus indicating that the ions have not fully returned to their initial distribution in the absence of a temperature gradient. Specifically, a portion of the Na^+ ions remain localized near the cold end. This phenomenon can be attributed to the formation of an electric double layer, wherein the negative charges on the cold-end electrode interact with Na^+ ions to create a stable, low-capacitance electric double-layer structure. This persistent ion-electrode interaction poses a challenge to achieving full ion redistribution, thereby slightly reducing the energy conversion efficiency of the ITEC device. Nevertheless, as shown in Figure 6c, the PVA$\alpha_{0.12}$/$I_{0.3}$ sample demonstrates excellent sensitivity and reproducibility to variations in the temperature gradient over an extended period of 10 000 s. Notably, the device maintains its high sensitivity to temperature fluctuations, even after prolonged operation under ambient atmospheric conditions, with minimal degradation in thermopower. These results indicate that the PVA/α-CD/NaI hydrogel system developed herein possesses significant potential as a self-powered temperature sensor, and is capable of sustained performance over time. However, it is important to note that maintaining long-term stability of ionic thermoelectric performance under ambient conditions necessitates exterior packaging to prevent water loss and preserve mechanical integrity.

The power density supplied by the device at specific resistances can be calculated by plotting the potential difference against time during Stage II and integrating the resulting curve, in accordance with Equation (5):

$$P = \frac{E}{\Delta t} = \int_0^{\Delta t} \frac{V^2}{AR} dt \quad (5)$$

where E represents the energy density, Δt is the duration of the charging process, V is the potential difference, A is the cross-sectional area of the hydrogel, and R is the external resistance. When the external resistance decreases, the current loss is minimized, thus resulting in an optimized power density of 5.9 mW m^{-2} (Figure 6d). This trend is consistent with the previous report.[55,56] The significant power density highlights the promising potential of the PVA$\alpha_{0.12}$/$I_{0.3}$ sample for application in ITEC devices.

To further enhance the voltage output and expand the application potential of the ITEC, a 3-leg ITEC module was fabricated by connecting multiple PVA$\alpha_{0.12}$/$I_{0.3}$ hydrogels in a zigzag configuration, as shown in **Figure** 7a. In this configuration, the PVA$\alpha_{0.12}$/$I_{0.3}$ hydrogel blocks, each cut to dimensions of 1.5 × 1.5 × 0.3 cm^3, were encapsulated within flexible PDMS molds. Carbon cloth electrodes were attached to both the top and bottom surfaces, with PI tape securing the setup to ensure optimal contact

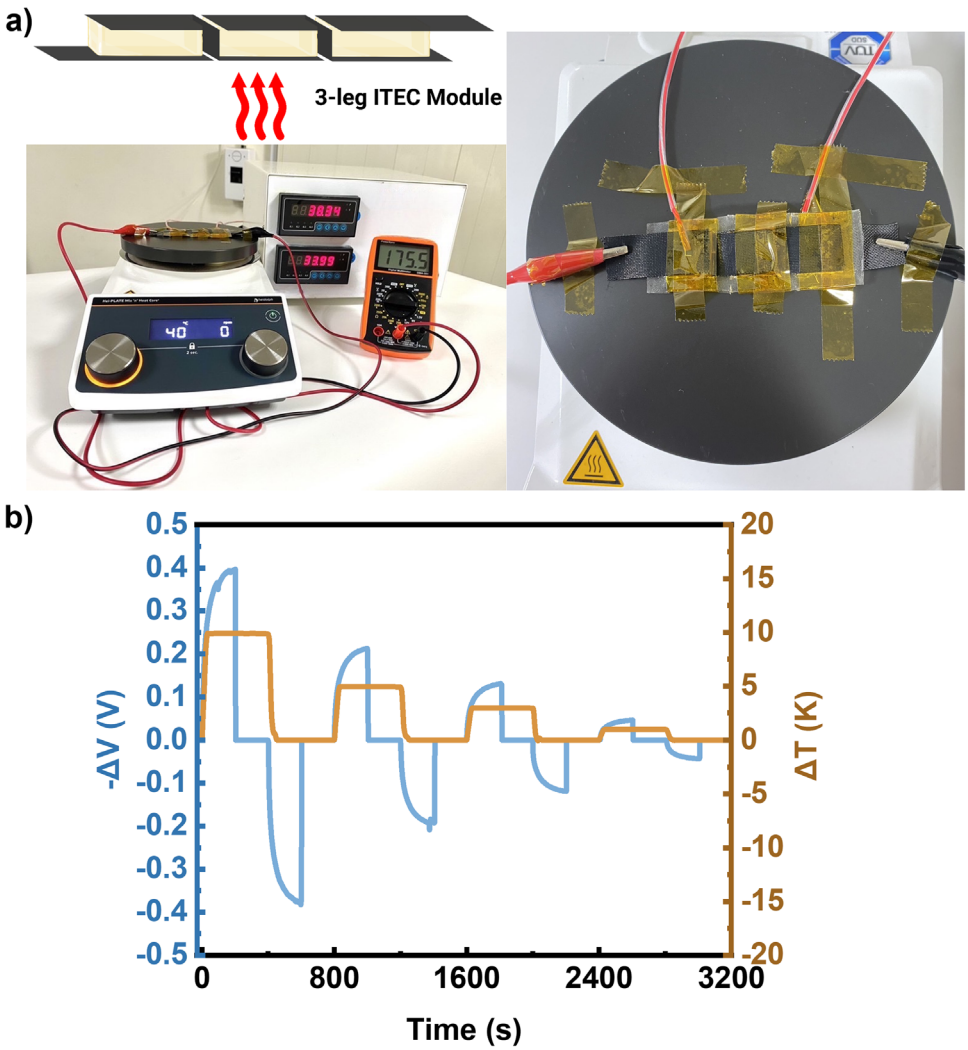

Figure 7. a) The illustrated figure and the actual device of the 3-leg ITEC module. b) The voltage-time and temperature-time profile for repeated four-stage charge–discharge tests.

between the hydrogel and the electrodes. When the 3-leg ITEC module was placed on a hotplate at 40 °C, it maintained a temperature difference of 4.4 K between the hot and cold ends, thereby generating a thermoelectric voltage of ≈176 mV (Figure 7a). A subsequent four-stage charge–discharge test, conducted at varying temperatures, yielded a thermoelectric voltage of 0.4 V at a temperature difference of ≈10 K (Figure 7b). Throughout the testing process, the ITEC module exhibited excellent stability and reproducibility. These remarkable thermoelectric properties suggest that the as-developed PVA$\alpha_{0.12}$/$I_{0.3}$ hydrogels hold significant promise as energy storage components for wearable devices, offering efficient and stable thermoelectric performance.

The PVA/α-CD/NaI hydrogel proposed in this study achieves notable thermopower and power factors under laboratory conditions, along with a certain degree of thermoelectric stability. Additionally, the material shows promise for applications in wearable electronic devices due to its excellent mechanical properties and stable voltage output over extended periods. To address the challenge of solvent volatility within the hydrogel, encapsulation with polymers such as PDMS is suggested to enhance device stability under ambient conditions.

3. Conclusion

In this study, a PVA/α-CD/NaI hydrogel system was successfully developed as a p-type thermoelectric capacitor (ITEC) by utilizing the supramolecular host–guest complexation between α–cyclodextrin (α-CD) and triiodide ions (I_3^-). This study represents the first application of host–guest complexation in the field of ITECs. Unlike approaches that rely on complexation between metal ions and ionic liquids involving concerns about biotoxicity, this research utilizes α-cyclodextrin and triiodide ions as host–guest complexation materials, offering superior advantages in terms of environmental friendliness, biocompatibility, and cost-effectiveness. Comprehensive characterization via FTIR, ^{13}C-NMR, UV–vis, and XPS techniques confirmed the chemical composition and the nature of the host–guest interactions within the hydrogel matrix. The thermoelectric properties,

including thermopower, ionic conductivity, and thermal conductivity, were systematically investigated across various concentrations of α-CD and NaI. The results demonstrated that host–guest complexation significantly enhances the thermoelectric performance by effectively restricting the diffusion of I_3^- ions within the hydrogel matrix. Among the tested samples, the PVA$\alpha_{0.12}$/$I_{0.3}$ achieved the highest thermopower of 14.24 mV K^{-1}, along with an ionic power factor of 477.2 μW K^{-2} m^{-1}. The optimal performance was achieved when the concentration of α-CD aligned with the effective concentration of I_3^-, underscoring the importance of a balanced complexation for maximizing the thermoelectric efficiency. Furthermore, microstructural analysis revealed that the inclusion of α-CD improved the mechanical properties of the PVA hydrogel, making it more suitable for stretchable and wearable device applications. The hydrogels also maintained a high sensitivity to temperature fluctuations and displayed excellent thermal stability. Overall, this study establishes the feasibility of enhancing p-type thermoelectric materials via the strategic manipulation of α-CD and I_3^- interactions, thereby offering a promising pathway for the development of advanced ITECs. These findings contribute valuable insights for future research in thermoelectric energy conversion and open up new avenues for the integration of supramolecular chemistry into functional materials design.

4. Experimental Section

Materials: Poly(vinyl alcohol) (>99.0%, fully hydrolyzed, M_w = 148000) and glutaraldehyde (25% aqueous solution) were purchased from Sigma–Aldrich Co. (USA). α-Cyclodextrin (>98.0%), β-cyclodextrin (>98.0%), γ-cyclodextrin (>98.0%), hydrochloric acid (36.5-38.0%), sodium iodide (>99.0%), sodium chloride (>99.0%) were purchased from Tokyo Chemical Industry Co. (Japan). All chemicals were used as received without any purification or treatment.

Preparation of PVA/α-CD/NaI Hydrogels: Initially, a 10 mL PVA/α-CD solution was prepared by dissolving 1.0 g of PVA and 0/0.389/0.778/1.167 g of α-CD in deionized water at 90 °C with continuous stirring for 24 h as illustrated in Figure S1 (Supporting Information). The solution was then cooled to 25 °C, and any bubbles were removed using a vacuum desiccator. Concurrently, a 0.1 M hydrochloric acid solution was prepared to act as a catalyst for the crosslinking reaction. Using a microdropper, 0.5 mL of the hydrochloric acid solution and 0.15 mL of glutaraldehyde solution were slowly added to the vial while maintaining the temperature at 90 °C and stirring until the mixture was homogeneous. The resulting mixture was poured into a square mold made of PTFE and maintained at 80 °C for ≈30 min to complete the crosslinking process. Once the solid-state hydrogel was formed, it was submerged in sodium iodide solutions of varying concentrations for 24 h before conducting thermoelectric property measurements and various spectral analyses.

Thermoelectric Properties Measurement: All thermopower (S_i) measurements in this paper were performed using the custom-built thermoelectric measurement apparatus illustrated in Figure S13 (Supporting Information). Each sample for thermopower measurements was cut into $1 \times 1 \times 0.3$ cm^3. Both the cold and hot end electrodes were made of carbon cloth. The cold end temperature was maintained at 25 ± 1 °C using a water chiller equipped with a pump, while the hot end temperature was adjusted using an electric heating control device. The thermovoltage was measured by Keithley 2182A. During the measurements, the ionic hydrogel was stabilized for 5 min at each point to ensure ion diffusion equilibrium. For each temperature difference, 15 data points were recorded. To determine the ionic conductivity of hydrogels, the bulk resistance was obtained via the electrochemical impedance spectroscopy (EIS) method and the ionic conductivity (σ_i) was then calculated using the formula: $\sigma_i = L/(A \times R)$, where L is the thickness of the hydrogel sample, A is the cross-sectional area of the hydrogel sample and R is the obtained bulk resistance. The EIS measurements were conducted with BioLogic SP-150e potentiostat in which the voltage amplitude was set to be 10 mV and the frequency ranges from 1 MHz to 10 mHz. Platinum was used as the electrode material for these measurements. The measurement of thermal conductivity (κ) was conducted using the transient plane source (TPS) method, utilizing a Hot Disc TPS 2500S thermal constant analyzer with the bulk module.

Characterization: The cross-sectional microstructure of the freeze-dried hydrogels was examined using scanning electron microscopy (SEM, JEOL JSM-6510) at an acceleration voltage of 15 kV. Prior to SEM imaging, the hydrogels were freeze-dried for 72 h and sputter-coated with Pt. FTIR analyses were performed with a PerkinElmer Spectrum Two FT-IR L16000 apparatus, while UV–vis spectra were obtained using a Hitachi U-4100 UV–vis–NIR spectrophotometer. For the freeze-dried hydrogel samples, $_{13}$C-NMR experiments were carried out using a Bruker Avance III 600 MHz solid-state NMR. Tensile stress–strain curves were measured with a SHIMADZU EZ-Test Universal Testing Machine at a stretching rate of 2 mm min^{-1}, with the hydrogel samples cut into dimensions of $1 \times 3 \times 0.3$ cm^3. The X-ray diffraction plot was acquired using a Rigaku MiniFlex X-ray Diffractometer with the hydrogel drop-cast onto a glass substrate. Dynamic mechanical analyses were performed with TA Instruments HR-2 System Rheometer. Gel-state X-ray photoelectron spectroscopy (XPS) experiments were performed at the TLS 24A Beamline of the National Synchrotron Radiation Research Center (NSRRC), while small-angle X-ray scattering (SAXS) measurements were carried out at the NSRRC's TPS 13A Beamline. Data analysis, including model fitting and linear fitting, was carried out using IGOR Pro 6.10A.

Supporting Information

Supporting Information is available from the Wiley Online Library or from the author.

Acknowledgements

This work was supported by the Undergraduate Research Fellowship Program by the National Science and Technology Council (NSTC) in Taiwan (under grant 112CFA0100117), and the Advanced Research Center for Green Materials Science and Technology from The Featured Area Research Center Program within the framework of the Higher Education Sprout Project by the Ministry of Education (112L9006). The authors thank Beamline TLS 24A1 and TPS 13A from the National Synchrotron Radiation Research Center (NSRRC) of Taiwan for providing beamline. The authors acknowledge support from the 2030 Cross-Generation Young Scholars Program funded by the National Science and Technology Council (NSTC) in Taiwan (NSTC 113-2628-E-002-028), the Academic Research—Career Development Project (Sprout Research Projects) funded by National Taiwan University (NTU113L7839)

Conflict of Interest

The authors declare no conflict of interest.

Data Availability Statement

The data that support the findings of this study are available from the corresponding author upon reasonable request.

Keywords

host–guest complexation, hydrogel, ionic thermoelectrics, low-grade heat harvesting, supramolecular chemistry, thermopower

Received: November 24, 2024
Revised: December 26, 2024
Published online: January 22, 2025

[1] Y. Tian, X. Yang, K. Li, Q. Zhang, Y. Li, H. Wang, C. Hou, *Mater. Today Energy* **2023**, *36*, 101342.
[2] H. Cheng, Q. Le, Z. Liu, Q. Qian, Y. Zhao, J. Ouyang, *J. Mater. Chem. C* **2022**, *10*, 433.
[3] N. Jabeen, M. Muddasar, N. Menéndez, M. A. Nasiri, C. M. Gómez, M. N. Collins, R. Muñoz-Espí, A. Cantarero, M. Culebras, *Chem. Sci.* **2024**, *15*, 14122.
[4] R. Xiao, X. Zhou, C. Zhang, X. Liu, S. Han, C. Che, *Sensors* **2024**, *24*, 4600.
[5] S. Lee, S. Kim, A. Pathak, A. Tripathi, T. Qiao, Y. Lee, H. Lee, H. Y. Woo, *Macromol. Res.* **2020**, *28*, 531.
[6] Y. Liu, H. Wang, P. C. Sherrell, L. Liu, Y. Wang, J. Chen, *Adv. Sci.* **2021**, *8*, 2100669.
[7] S. Sun, M. Li, X.-L. Shi, Z.-G. Chen, *Adv. Energy Mater.* **2023**, *13*, 2203692.
[8] M. Gao, P. Wang, L. Jiang, B. Wang, Y. Yao, S. Liu, D. Chu, W. Cheng, Y. Lu, *Energy Environ. Sci.* **2021**, *14*, 2114.
[9] D. Zhao, A. Würger, X. Crispin, *J. Energy Chem.* **2021**, *61*, 88.
[10] S. Jia, W. Qian, P. Yu, K. Li, M. Li, J. Lan, Y.-H. Lin, X. Yang, *Mater. Today Phys.* **2024**, *42*, 101375.
[11] Y.-H. Pai, J. Tang, Y. Zhao, Z. Liang, *Adv. Energy Mater.* **2023**, *13*, 2202507.
[12] Y. Han, H. Wei, Y. Du, Z. Li, S.-P. Feng, B. Huang, D. Xu, *Adv. Sci.* **2023**, *10*, 2302685.
[13] Y.-H. Pai, C. Xu, R. Zhu, X. Ding, S. Bai, Z. Liang, L. Chen, *Adv. Mater.* **2024**, 2414663.
[14] T. Li, X. Zhang, S. D. Lacey, R. Mi, X. Zhao, F. Jiang, J. Song, Z. Liu, G. Chen, J. Dai, Y. Yao, S. Das, R. Yang, R. M. Briber, L. Hu, *Nat. Mater.* **2019**, *18*, 608.
[15] B. Chen, Q. Chen, S. Xiao, J. Feng, X. Zhang, T. Wang, *Sci. Adv.* **2021**, *7*, eabi7233.
[16] Z. Liu, H. Cheng, Q. Le, R. Chen, J. Li, J. Ouyang, *Adv. Energy Mater.* **2022**, *12*, 2200858.
[17] Z. A. Akbar, J.-W. Jeon, S.-Y. Jang, *Energy Environ. Sci.* **2020**, *13*, 2915.
[18] H. Cheng, X. He, Z. Fan, J. Ouyang, *Adv. Energy Mater.* **2019**, *9*, 1901085.
[19] Q. Chen, B. Chen, S. Xiao, J. Feng, J. Yang, Q. Yue, X. Zhang, T. Wang, *ACS Appl. Mater. Interfaces* **2022**, *14*, 19304.
[20] W. Zhao, Y. Zheng, M. Jiang, T. Sun, A. Huang, L. Wang, W. Jiang, Q. Zhang, *Sci. Adv.* **2023**, *9*, eadk2098.
[21] J. Hu, J. Wei, J. Li, L. Bai, Y. Liu, Z. Li, *Energy Environ. Sci.* **2024**, *17*, 1664.
[22] S. B. Khan, S.-L. Lee, *Molecules* **2021**, *26*, 3995.
[23] M. Sayed, H. Pal, *Phys. Chem. Chem. Phys.* **2021**, *23*, 26085.
[24] A. Cid-Samamed, J. Rakmai, J. C. Mejuto, J. Simal-Gandara, G. Astray, *Food Chem.* **2022**, *384*, 132467.
[25] J. Zhang, H. Qiu, T. He, Y. Li, S. Yin, *Front. Chem.* **2020**, *8*, 560.
[26] R. Nag, C. P. Rao, *Chem. Commun.* **2022**, *58*, 6044.
[27] J.-u. Lee, S.-S. Lee, S. Lee, H. B. Oh, *Molecules* **2020**, *25*, 4048.
[28] B. Rajbanshi, S. Saha, K. Das, B. K. Barman, S. Sengupta, A. Bhattacharjee, M. N. Roy, *Sci. Rep.* **2018**, *8*, 13031.
[29] J. Szejtli, *Chem. Rev.* **1998**, *98*, 1743.
[30] M. Arslan, R. Sanyal, A. Sanyal, *Polym. Chem.* **2020**, *11*, 615.
[31] J. L. Pursell, C. J. Pursell, *J. Phys. Chem. A* **2016**, *120*, 2144.
[32] M. Okuda, T. Hiramatsu, M. Yasuda, M. Ishigaki, Y. Ozaki, M. Hayashi, K. Tominaga, E. Chatani, *J. Phys. Chem. B* **2020**, *124*, 4089.
[33] H. Zhou, T. Yamada, N. Kimizuka, *J. Am. Chem. Soc.* **2016**, *138*, 10502.
[34] M. Pooresmaeil, H. Namazi, *Polym. Adv. Technol.* **2019**, *30*, 447.
[35] K.-J. Kim, S.-B. Lee, N.-W. Han, *Korean J. Chem. Eng.* **1994**, *11*, 41.
[36] Z. Xue, D. He, X. Xie, *J. Mater. Chem. A* **2015**, *3*, 19218.
[37] J. Jortner, M. Ottolenghi, G. Stein, *J. Phys. Chem.* **1962**, *66*, 2042.
[38] G. Braathen, P. T. Chou, H. Frei, *J. Phys. Chem.* **1988**, *92*, 6610.
[39] D. Ghemati, D. Aliouche, *J. Appl. Spectrosc.* **2014**, *81*, 257.
[40] H. S. Mansur, C. M. Sadahira, A. N. Souza, A. A. P. Mansur, *Mater. Sci. Eng., C* **2008**, *28*, 539.
[41] H. Wang, M. Guo, Y. Wu, J. Zhang, S. Xue, X. Yang, Z. Li, *Mater. Res. Express* **2020**, *7*, 065307.
[42] J. Joseph, E. D. Jemmis, *J. Am. Chem. Soc.* **2007**, *129*, 4620.
[43] F. Adrian, T. Budtova, E. Tarabukina, M. Pinteala, S. Mariana, C. Peptu, V. Harabagiu, B. C. Simionescu, *J. Inclusion Phenom. Macrocyclic Chem.* **2009**, *64*, 83.
[44] S. V. Kireev, S. L. Shnyrev, *Laser Phys.* **2015**, *25*, 075602.
[45] Y. Bai, L. Ye, L. Wang, X. Shi, P. Wang, W. Bai, P. K. Wong, *Appl. Catal., B* **2016**, *194*, 98.
[46] G. Beaucage, *J. Appl. Crystallogr.* **1996**, *29*, 134.
[47] S. Prevost, T. Lopian, M. Pleines, O. Diat, T. Zemb, *J. Appl. Crystallogr.* **2016**, *49*, 2063.
[48] G. Beaucage, *J. Appl. Crystallogr.* **1995**, *28*, 717.
[49] D. McDowall, D. J. Adams, A. M. Seddon, *Soft Matter* **2022**, *18*, 1577.
[50] C.-M. Tang, Y.-H. Tian, S.-H. Hsu, *Materials* **2015**, *8*, 4895.
[51] M. L. V. Ramires, C. A. Nieto de Castro, Y. Nagasaka, A. Nagashima, M. J. Assael, W. A. Wakeham, *J. Phys. Chem. Ref. Data* **1995**, *24*, 1377.
[52] Q. Chen, B. Cheng, Z. Wang, X. Sun, Y. Liu, H. Sun, J. Li, L. Chen, X. Zhu, L. Huang, Y. Ni, M. An, J. Li, *J. Mater. Chem. A* **2023**, *11*, 2145.
[53] W. Zhao, Y. Zheng, A. Huang, M. Jiang, L. Wang, Q. Zhang, W. Jiang, *Adv. Mater.* **2024**, *36*, 2402386.
[54] B. Chen, J. Feng, Q. Chen, S. Xiao, J. Yang, X. Zhang, Z. Li, T. Wang, *npj Flexible Electron.* **2022**, *6*, 79.
[55] Y. Fang, H. Cheng, H. He, S. Wang, J. Li, S. Yue, L. Zhang, Z. Du, J. Ouyang, *Adv. Funct. Mater.* **2020**, *30*, 2004699.
[56] M. Fu, Z. Sun, X. Liu, Z. Huang, G. Luan, Y. Chen, J. Peng, K. Yue, *Adv. Funct. Mater.* **2023**, *33*, 2306086.